Volume 1 | Number 1 | Jan 2013 | Pages 1–100

Nanoscale

www.rsc.org/nanoscale

ROYAL SOCIETY OF CHEMISTRY

This is an *Accepted Manuscript*, which has been through the Royal Society of Chemistry peer review process and has been accepted for publication.

Accepted Manuscripts are published online shortly after acceptance, before technical editing, formatting and proof reading. Using this free service, authors can make their results available to the community, in citable form, before we publish the edited article. We will replace this *Accepted Manuscript* with the edited and formatted *Advance Article* as soon as it is available.

You can find more information about *Accepted Manuscripts* in the **Information for Authors**.

Please note that technical editing may introduce minor changes to the text and/or graphics, which may alter content. The journal's standard **Terms & Conditions** and the **Ethical guidelines** still apply. In no event shall the Royal Society of Chemistry be held responsible for any errors or omissions in this *Accepted Manuscript* or any consequences arising from the use of any information it contains.

Journal Name

ARTICLE TYPE

Engineering the nanostructure of a polymer-nanocomposite film containing Ti-based core-shell particles to enhance dielectric response[†]

Amoghavarsha Mahadevegowda,[*] Neil P Young, and Patrick S Grant

Nylon-6 based polymer-nanocomposite (PNC) dielectrics containing nano-regions of Ti-only and Ag+Ti have been manufactured by layer-by-layer deposition. By varying the thickness and deposition rate of individual layers, the PNC structure was manipulated at the nano-scale and then studied using various types of transmission electron microscopy (TEM). Enhanced PNC dielectric properties, with a dielectric constant k as high as $\sim$73, were shown to relate critically to *in-situ* reactions and the detailed nano-arrangement of the resulting Ti (core)-TiO$_x$ (shell) and Ag nanoparticles.

1 Introduction

Polymer-nanocomposites (PNCs) have received interest for applications in high energy density capacitors, electromagnetic interference (EMI) shielding, actuators, sensors, and solar cells.[1–9] For dielectric applications in particular, researchers have sought to exploit the enhancement in effective dielectric constant k observed around the current percolation threshold at a critical volume fraction of conducting nano-filler in what is often referred to as a "micro-capacitor network effect".[6,10–17] However, this effect can be difficult to implement over the large areas needed for practical devices because of the need to impose strict control of the volume fraction v_f of filler phase to just below the percolation threshold at all points during processing. A subsequent

development of this approach introduces an additional interface or "interphase" as a discreet third layer of material separating the nano-filler and the matrix, usually through the use of core-shell nanoparticles, which facilitate charge storing/trapping at the core/shell and shell/matrix interfaces and thereby enhance the interfacial polarisability.[18–24] In core-shell particulate fillers, the outer "shell" fulfils the role of the interphase and when an insulator, can also inhibit excessive current percolation effects.

In previous work we employed successfully a simple and scalable vacuum deposition technique to fabricate high-k Al (core)-oxide (shell) nanoparticles containing PNCs with carefully controlled nanostructures and dielectric constants of up to 29 at 1 kHz.[21] We now extend and enhance this approach in two ways. Firstly, since we showed that the nature of the shell affects the overall effective dielectric properties,[21] the choice of the particulate phase that undergoes *in-situ* oxidation to form the oxide-shell, is crucial. A rational choice of metal would be a reac-

Department of Materials, University of Oxford, Parks Road, Oxford, OX1 3PH, UK; E-mail: amogh.gowda@materials.ox.ac.uk

tive metal that naturally forms a semiconducting, high-k oxide-shell, [19] such as Ti where TiO_2 is, in bulk at least, semiconducting and highly-polarisable with k in the range 12-114, spanning amorphous TiO_2 to crystalline TiO_2 (anatase and rutile, both tetragonal). [25–30]

Secondly we now also incorporate a *conducting*, non-oxidising secondary phase using evaporated Ag as discrete, non-continuous islands sandwiched by polymer layers to provide an additional virtuous contribution to the effective k of the device via the near-percolation micro-capacitor network effect. [6,10–17] Rather than mixing the Ag throughout the polymer as is usually done, and which leads to problems of excessive percolation and break-down previously mentioned, we control the relative thickness of very thin discrete polymer and metallic layers with more lo-calised regions of inter-mixing. Scanning transmission electron microscopy (STEM), selected area electron diffraction (SAED) and high-resolution TEM (HRTEM) are used to study the structure and chemistry of the PNC films showing enhanced or "super-k" behaviour, which are then explained in terms of the detailed nano-arrangement of Ti and Ag+Ti based particles in the nylon-6 matrix.

2 Results and discussion

Ti and nylon-6 based samples are referred to as Ti_i-Ny_t where the subscripts i and t are variables which denote the deposition rate of Ti and the final thickness of the nylon-6 layer respectively (see the Experimental section for full details).

Figure 1 shows the variation of dielectric constant (▲) and dis-sipation factor (●) of the $Ti_{0.5}$-Ny_{20} PNCs as a function of thick-ness t of the deposited Ti layer at 1 kHz and 40 ^{0}C (an elevated temperature was used to ensure the films were dry and to mini-mize the contribution of any water molecules to the effective di-electric constant). The dielectric constant increased dramatically from ∼4 for nylon-6 only to ∼26 at a Ti layer of t=5 nm, and then to ∼38 at t=10 nm. The dissipation factor $tan\ \delta$ increased from ∼0.19 for nylon-6 only to ∼0.32 for both Ti-PNCs. Both k and tan δ of the Ti-PNCs were higher than those of similarly processed Al-PNCs [21,31] at all nominal thicknesses of the Ti layer, presumably
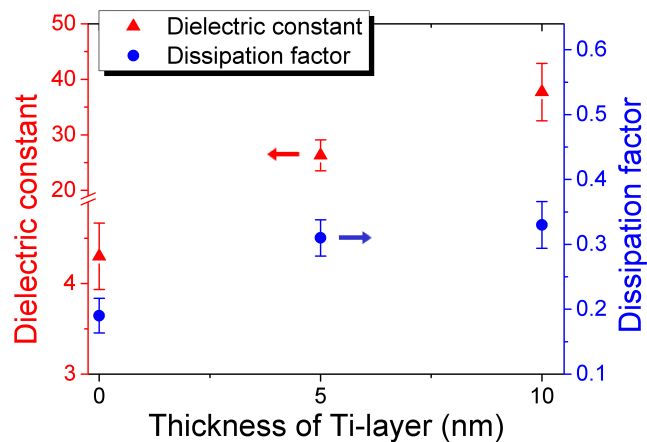

Fig. 1 Variation of dielectric constant (▲) and dissipation factor (●) of the $Ti_{0.5}$-Ny_{20} PNCs with thickness of the deposited Ti layer at 1 kHz and 40 ^{0}C.

due to the formation of inherently more lossy Ti-based oxides.

Annular dark field (ADF)-STEM images of the $Ti_{0.5}$-Ny_{20} PNCs for the Ti layer t=5 and 10 nm are shown in Figure 2(a) and (c) respectively; the corresponding SAED patterns are shown in Fig-ure 2(b) and (d) respectively with diffraction rings in the SAED patterns more apparent in the corresponding enhanced images in Figure 2(e) and (f). In general, the deposited Ti showed good "wetting" onto the prior nylon-6 layer, similar to Al [21,31] and as shown in Figure 2(a) and (c). The SAED patterns showed diffrac-tion rings due to crystalline phases, highlighted in Figure 2(a) and (c), which were continuous and relatively thick, suggesting the presence of many randomly oriented, small crystals.

The measured d-spacing from the first ring in Figure 2(f) was in the range 0.35-0.36 nm and suggested to correspond to the (101) plane of TiO_2-anatase with a d-spacing of ∼0.351 nm. [32] The measured d-spacings from the second and third rings were in the range 0.24-0.21 nm and 0.15-0.13 nm respectively, and again show close approximation to both anatase [33] and Ti. [34] The diffraction rings in Figure 2(f) were brighter than the ones in Fig-ure 2(e) due to an overall increase in the fraction and size of Ti-based crystalline nanoparticles in the PNC with t_{Ti}=10 nm when compared with t_{Ti}=5 nm PNC. This possibility is also supported by the presence of relatively large, highly diffracting crystals (en-circled) in Figure 2(c) where t_{Ti}=10 nm. The close overlapping of diffraction rings limited further meaningful analysis that might

yield more detailed information pertaining to the crystal chemistry and structure. Overall, the formation of both a Ti-based oxide and some residual metallic Ti at nominal deposited Ti thicknesses of $t=5$ and 10 nm was suggested.
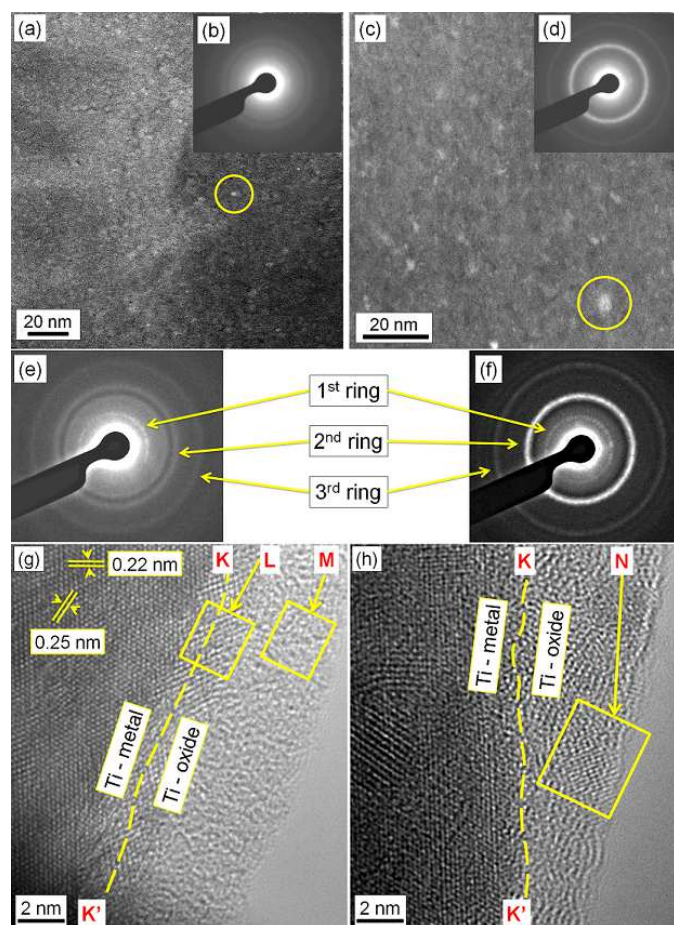
Fig. 2 ADF-STEM images [(a) and (c)] and the corresponding SAED patterns [(b) and (d)] of $Ti_{0.5}$-Ny_{20} PNCs at nominal Ti thicknesses of $t=5$ and 10 nm respectively; (e) and (f) are the enhanced images of the SAED patterns, (b) and (d). The highlighted regions in (a) and (c) are highly diffracting Ti-based crystals. (g) and (h) are HRTEM images of two different Ti-nanoparticles showing a Ti-oxide (shell) and a Ti-metal (core) from a Ti-only PNC at $t_{Ti}=10$ nm. The superimposed line KK' is an approximate, indicative boundary between the Ti-metal (core) and Ti-oxide (shell). A highly-defective nanostructure, highlighted in box L, coincided with the indicative boundary, where the structure makes a transition from crystalline metal to amorphous oxide (highlighted in box M). A region of short-range order in the amorphous oxide shell of (h) is highlighted in box N.

HRTEM images of two different Ti-based nanoparticles showing a Ti-oxide (shell) and a Ti-metal (core) from a Ti-PNC with a nominal Ti thickness of $t=10$ nm are shown in Figure 2(g) and (h), taken from regions near the edges of Ti-nanoparticles (for example, a Ti-based core-shell nanoparticle protruding into vacuum is shown in Figure S1(a), Supporting Information). The measured d-spacings from the crystalline region were 0.25 nm and 0.22 nm and corresponded to $(01\bar{1}0)$ and $(01\bar{1}1)$ lattice planes of Ti respectively. The superimposed line AA' is an approximate, indicative boundary between the Ti-metal (core) and Ti-oxide (shell). A typical highly-defective nanostructure in the shell region is highlighted in box L, where the structure makes a transition from the crystalline Ti-metal to an amorphous Ti-oxide. In Figure 2(h), there were regions of short-range order (for example, in the highlighted box N) within the amorphous-like oxide-shell. Since the stoichiometry of the Ti-oxide shell could not be measured accurately, it is subsequently referred to as TiO_x.

Returning to the high k behaviour in Figure 1, once a Ti layer was introduced into the nylon-6, the elevation in k cannot be attributed simply to the subsequent formation of anatase ($k=47$[26]) through a law of mixtures approach because the measured value of $k\sim38$ would require an anatase volume fraction of ~0.8, instead of the actual fraction of ~0.2 (which is the maximum that can be assumed if all the deposited Ti transformed to anatase). Even when the full range of dielectric constants for anatase or various other amorphous Ti-oxides are considered,[25–29] which lie in the range 40-48 and 12-18 respectively, there is no support for a simple mixing rule approach to explain the elevated dielectric constant. Therefore, consistent with earlier Al-PNC behaviour, the enhancement in k in Figure 1 was ascribed to the presence of the relatively polarisable Ti (core)-TiO_x (shell) nanoparticles and the associated introduction of a defective and likely non-stoichiometric oxide shell that facilitates additional charge separation mechanisms.[21]

## 2.1 Effect of adding Ag nanoparticles and changing the Ti deposition rate

In order to enhance the polarisability of all the material between the capacitor plates, very thin layers of Ag were deposited into the nylon-6 layers that sandwiched the region of TiO_x and Ti particles, with the intent that the resulting Ag nanoparticles might create a high-k near-percolation network in the nylon-6.

Figure 3 shows the variation of (a) dielectric constant and (b) dissipation factor of Ti-PNCs and Ag+Ti-PNCs as a function of the
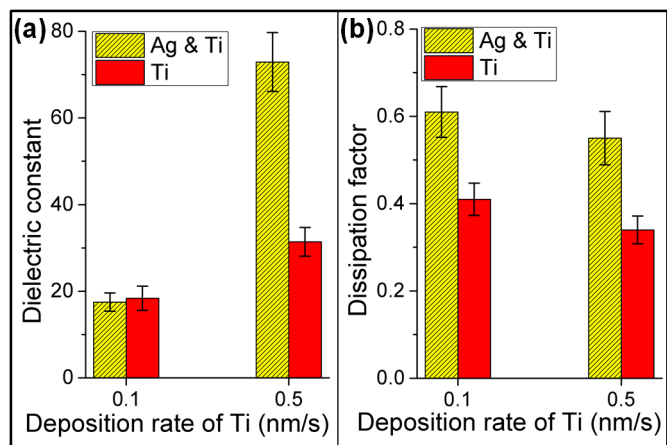
Fig. 3 The variation of (a) dielectric constant and (b) dissipation factor of Ti-PNCs and Ag+Ti-PNCs with deposition rate of Ti at 1 kHz and 40 ^{0}C. The thicknesses of the nominally discrete deposited Ti, nylon-6 and Ag layers in all the PNCs were 10, 10 and 5 nm respectively.

deposition rate of Ti in the range 0.1 to 0.5 nm/s at 1 kHz and 40 ^{0}C. The final thicknesses (measured *in-situ* by a quartz crystal monitor) of the nominally discrete deposited Ti, nylon-6 and Ag layers in all the PNCs were 10, 10 and 5 nm respectively (although as shown later, some inter-mixing took place). A Ti-PNC with i_{Ti}=0.5 nm/s gave k~31 and was significantly higher than k~18.5 for Ti-PNCs with i_{Ti}=0.1 nm/s, although the dissipation factor was similar in the range 0.34-0.41.
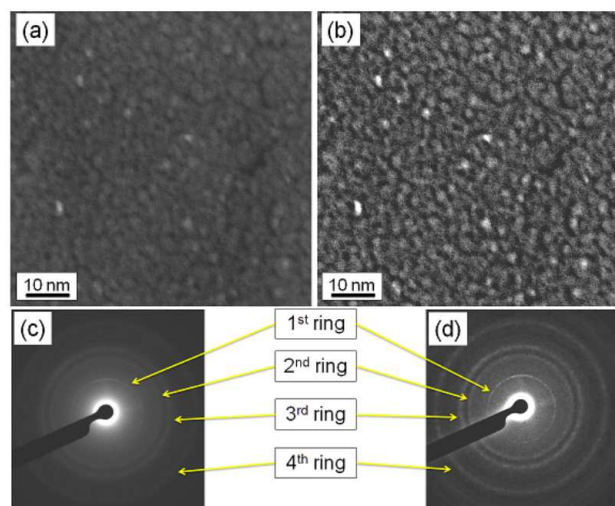

Fig. 4 (a) ADF-STEM image and (c) the corresponding SAED pattern of a Ti$_{0.1}$-Ny$_{10}$ PNC film; (b) and (d) are the enhanced images of (a) and (c) respectively.

Figure 4(a) and (c) show the ADF-STEM image and the corresponding SAED pattern of a Ti$_{0.1}$-Ny$_{10}$ PNC film respectively, while Figure 4(b) and (d) are the enhanced images of Figure

Table 1 The measured *d*-spacings from the SAED pattern in Figure 4 and the closest matches from anatase and Ti.

Ring #	d (nm)	Anatase (hkl)	Ti (hkil)
1	~0.36	(101)	X
2	0.23-0.25	(103), (004), (112)	(01$\bar{1}$0)
3	0.20-0.22	(200)	(01$\bar{1}$1)
4	0.14-0.15	(211), (105)	(11$\bar{2}$0)

4(a) and (c) respectively. The ADF-STEM image showed bright Ti-islands in a dark nylon-6 matrix. The measured *d*-spacings from the SAED and the closest matches are shown in Table 1 and again both anatase-like TiO$_x$ and crystalline Ti were confirmed.
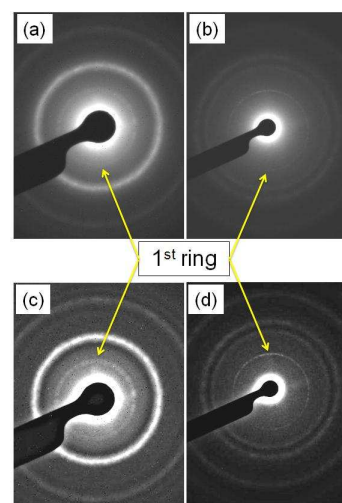
Fig. 5 SAED patterns of Ti-PNCs at i_{Ti}= (a) 0.5 nm/s and (b) 0.1 nm/s; (c) and (d) are the corresponding enhanced images of (a) and (b) respectively.

Figure 5(a) and (b) show the SAED patterns of Ti-PNCs at Ti deposition rates of i_{Ti}=0.5 and 0.1 nm/s respectively, and Figure 5(c) and (d) are the corresponding enhanced images. The first diffraction ring in Figure 5(c) was wider than that in Figure 5(d), suggesting that TiO$_x$ crystals formed at i_{Ti}=0.1 nm/s, corresponding to Figure 5(d), were larger than those formed at i_{Ti}=0.5 nm/s. Since the nominal thickness and overall fraction of Ti deposited was intended to be consistent at t=10 nm for both the deposition rates, one conclusion is that the fraction Ti transformed to TiO$_x$ was increased at the lower deposition rate, because formation of TiO$_x$ was, at least initially, an *in-situ* reaction involving residual O$_2$ in the evaporation chamber, and the very slow leakage of O$_2$ into the deposition chamber from ambient over longer deposition times (lower deposition rates) facilitated

a greater fraction of TiO_x. However, the presence of metallic Ti confirmed by TEM suggested that the amount of O_2 present in the chamber was not sufficient to fully oxidised all the evaporated Ti.

Figure 3 also shows that Ag+Ti-PNCs with i_{Ti}=0.1 nm/s had k∼17.5, which was comparable with k∼18.5 of Ti-PNCs at the same deposition rate. However, there was a dramatic increase to k∼73 for Ag+Ti-PNCs with i_{Ti}=0.5 nm/s, although as might be expected with an increased metallic fraction, both Ag+Ti-PNCs were more lossy, with $tan\ \delta$ approximately doubling to lie the range 0.55-0.61.

Figure 6(a) shows a ADF-STEM plan-view image of the three-phase Ag+$Ti_{0.5}$-Ny_{10} PNC film with Ag nanoparticles or nano-islands "sitting" over one another, with the intervening layers of nylon-6 and the Ti-rich layer in the centre of the device, between the two Ag containing layers. (To aid understanding, the reader may find it useful to refer also to schematic Figure 7(a) of this structure, which is explained in more detail subsequently, and Figure 8 in the appended "Experimental" section.) Figure 6(b) is a TEM image of a Ag+$Ti_{0.5}$-Ny_{10} PNC film and 6(c) is the corresponding SAED pattern. The measured d-spacings from the rings in the SAED pattern were: 0.24, 0.21, 0.15, and 0.12 nm corresponding to (111), (002), (022), and (113) lattice planes of Ag.[35] Any evidence of the presence of Ti or its oxide was not obvious from the unprocessed SAED pattern. Figure 6(d) is an enhanced image of Figure 6(c), while Figure 6(e) is the magnified region from the highlighted square shown in Figure 6(d). Figure 6(e) shows two faint rings which are marked as "first" and "second" rings. The measured d-spacings from these rings were ∼0.36 and ∼0.17 nm respectively, which did not belong to Ag, but may offer a match with TiO_2-anatase with (101)=0.351 nm, (105)=0.1699 nm, and (211)=0.1655, or Ti (01$\bar{1}$2)=0.1726 nm, suggesting the discrete presence of both metallic and oxidised Ti, along with the Ag nano-islands. Although d=0.17 nm was close to Ag_2O (220)=0.168 nm,[36] the absence of a ring corresponding to Ag_2O (110)=0.337 nm[36] undermined the case for the presence of Ag_2O, and anatase-like TiO_x was considered more likely, especially in terms of the previous results for Ag-only[11,31] and Ti-only containing films (see earlier).

During the deposition of a metal on a polymer, the metal atoms that impinge on the polymer surface can dissolve leading to the embedding of metal particles inside the polymer. This solubility of metal atoms is promoted at temperatures above the polymer glass transition temperature, where the polymer chains become mobile over comparatively long-range.[37,38] The measured temperature of the glass substrate during metal deposition of ∼40 ^{0}C was close to the glass transition temperature (T_g) of nylon-6 (reported in the range 43-49 ^{0}C[39]), although metallic atom embedding has also been observed at temperatures below the glass-transition temperature.[40] The constant temperature heat-treatment of the Ag+$Ti_{0.5}$-Ny_{10} PNC films to remove water-vapor effects also took place at ∼40 ^{0}C for 20 hours prior to dielectric measurement, and might have assisted further in the embedding or mobility of metal atoms: predominantly the metallic Ag atoms/nano-clusters since a majority of the Ti clusters can be expected to be already oxidised and less mobile by this stage. Further, the initial deposited layer of nylon-6 onto which the Ag, Al or Ti were then deposited was rough at the nano-scale so that incoming Ag, Al and Ti atoms form nano-islands or nanoparticles at varying heights or thicknesses across the cross-section of the nylon-6 film, not in a discrete, flat layer, and as observed in the TEM.

Based on these considerations, a proposed schematic representation of the Ag+$Ti_{0.5}$-Ny_{10} based PNC cross-section is shown in Figure 7(a). The Ag, Ti (core)-TiO_x (shell), and TiO_x nanoclusters are embedded/formed at different thicknesses across the cross-section of the nylon-6 film, according to their sequential deposition.

The majority of the Ag and Ti nano-clusters are within comparatively narrow layers, identified in Figure 7(a) as A and B respectively. The Ti-layer (B) has Ti (core)-TiO_x (shell) nanoparticles dispersed in a matrix that is comprised of *both* Ti-oxide (anatase-like TiO_x and amorphous TiO_x) as the majority phase and nylon-6 as the minority phase. Thus any two neighbouring nanoparticles with metallic Ti cores are separated by a thin layer of dielectric, either nylon-6 or TiO_x, or both. Such an arrangement results in the formation of an "internal boundary layer ca-
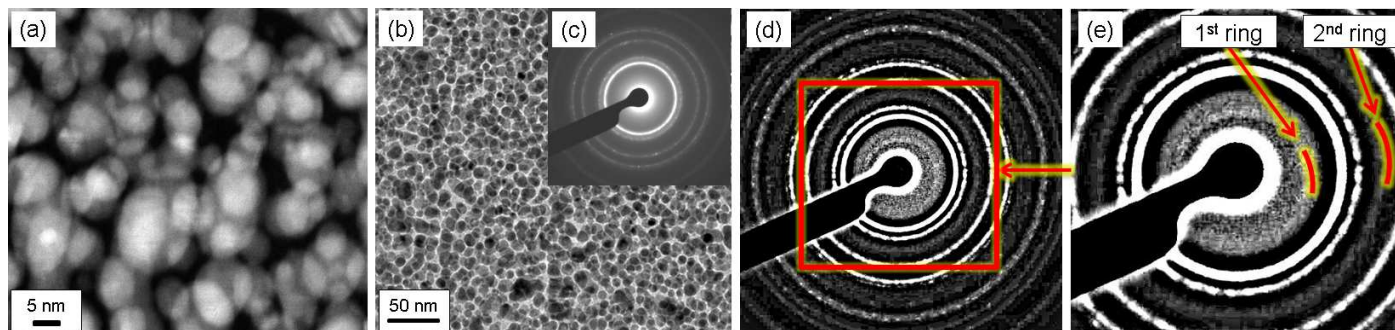
Fig. 6 (a) ADF-STEM image, (b) TEM image, and (c) the corresponding SAED pattern of a Ag+Ti$_{0.5}$-Ny$_{10}$ PNC film. (d) is an enhanced image of (c), and (e) is the magnified region from the highlighted square shown in (d).

pacitor" (IBLC).[41,42] Since the intervening layer of any dielectric between metallic electrodes is of the order of a few nanometers and a majority of the dielectric material in layer B is relatively high-k core-shell nanoparticles, an array of "nano-capacitors" or IBLCs that network randomly in series and parallel configurations is formed. This network, which is similar to a near-percolation network[6,10–17] but now consists of relatively polarisable core-shell particles in an insulating matrix, increases the effective k of the PNC.

The Ag layer (A) forms Ag nano-islands that function as metallic nano-electrodes with the nylon-6 ($k\sim4$)[43] as the dielectric between them. The Ag-network is a similar arrangement to the network of conducting particles in near-percolating composites[6,10–17] but with a change in the thickness of the nylon-6 layers between the Ag-clusters, as the local volume fraction of Ag changes as shown in Figure 7(a). The thickness of the dielectric (nylon-6) separating Ag-clusters is the lowest in the Ag-rich layer (A).

As explained earlier, there will always be a small fraction of Ag based clusters outside the narrow Ag-rich layers and these tiny, *conducting* clusters extend the region in which the nano-capacitor network effect operates to practically *the entire cross-section* of the film, from the top Al-electrode to the bottom. Thus the dielectric medium between the electrodes comprises nylon-6 containing Ag nano-islands, and Ti-based oxides and core-shell nanoparticles, close enough and sufficiently intermingled that a complex nano-capacitor network is established involving all the discrete phases. A cross-sectional schematic representation of this arrangement is

shown in Figure 7(b), which allowed the dielectric response to reach as high as $k\sim73$.

The effect of the nano-capacitor network was probed further by varying the thickness of the intervening nylon-6 layers with an intention to vary the effective volume fraction of Ag in the PNC. Figure 7(c) shows the variation of dielectric constant with thickness t_{Ny} of the deposited nylon-6 layer in Ti-PNC and Ag+Ti-PNC based capacitors at 40 ^{0}C and 1 kHz. The thicknesses of the deposited Ti and Ag layers in all PNCs were 10 and 5 nm respectively. In Figure 7(c) for Ti-PNCs with t_{Ny}=5 and 10 nm, k was almost the same at $k\sim20$ when the deposition of Ti was kept constant at i_{Ti}=0.1 nm/s. However, the Ag+Ti-PNC with a nylon-6 thickness of t=5 nm showed $k\sim29$, because of the increase in the effective volume fraction of Ag as shown in the schematic Figure S2 (see Supporting Information). These results further support the proposed explanation for super-k behaviour based on the formation of a single PNC containing mixed conducting and core-shell minority phases as described.

Three-phase, percolative PNC systems containing fillers such as BaTiO$_3$, Al and carbon-fibre[44,45] have shown k as high as 100 at 1 kHz, but the fillers in these PNCs are randomly mixed, which limits the control over the resulting dielectric properties especially over large areas, where as the present engineered nanocomposite structure ensures a thin insulating layer against the electrode. Moreover, the former PNCs require high-temperature processing (at 200 ^{0}C) or involve multi-step chemical synthesis routes, which are difficult to scale-up, and the thickness of the resulting films are in the range of μm-mm, limiting the overall enhancement
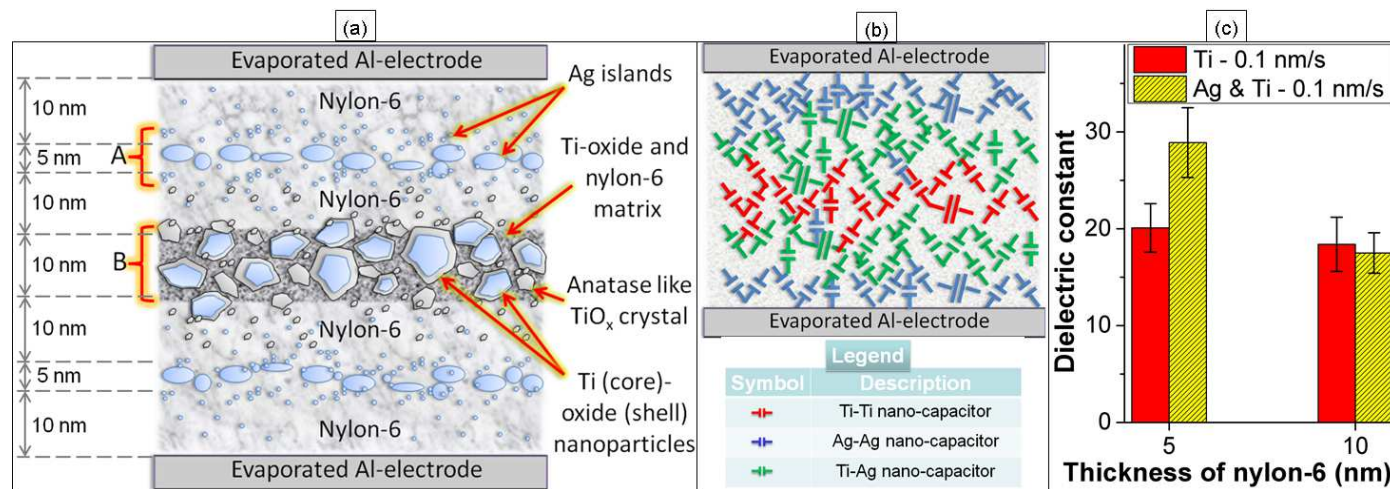
Fig. 7 (a) A cross-sectional schematic representation of a Ag+Ti$_{0.5}$-Ny$_{10}$ PNC based capacitor showing the nominal thickness of each layer of the dielectric, (b) the corresponding schematic showing different types of nano-capacitors that are randomly connected in parallel and series configurations resulting in a high-k dielectric, and (c) the variation of dielectric constant with thickness t of the deposited nylon-6 layer in Ti-PNC and Ag+Ti-PNC based capacitors at 1 kHz and 40 ^{0}C.

in absolute capacitances. We have employed a relatively simple, scalable, layer-by-layer deposition technique that involves a design-led approach, which places the fillers at discrete positions, to fabricate <100 nm thick, high-k PNC films.

3   Conclusions

A layer-by-layer deposition technique was used to fabricate Ti and Ti+Ag containing nylon-6 based high-k dielectrics. Studies involving STEM, SAED and HRTEM showed that the deposited Ti partially oxidised to form less polarisable Ti (core)-TiO$_x$ (shell) nanoparticles and in some cases, oxidised completely to form anatase nanoparticles. The TiO$_x$ shell showed both amorphous and semi-crystalline regions, and was studded with highly defective regions. Compared with nylon-6 alone, the high k of Ti-PNCs arose due to the combined contributions of the enhanced polarisability of core-shell and anatase-based nanoparticles. If a low Ti deposition rate was used, a relatively high volume fraction of anatase-based particles were formed in lower k-PNCs, suggesting that the enhancement in k was predominantly due to core-shell nanoparticles, and their associated enhanced interfacial polarisability effects.

Incorporating Ag nanoparticles and reducing the nylon-6 thickness to 10 nm resulted in a dielectric medium of inter-mingled Ag and Ti-based oxides and core-shell nanoparticles throughout

the nylon-6 matrix, despite nominally discrete layer deposition. The effective dielectric constant at 1 kHz was as high as $k \sim 73$ due to the combined effects of the polarisable Ti-based core-shell nanoparticles and a nano-capacitor network based interactions between all the discrete phases in a complex inter-connected nano-capacitor network. A decrease in the thickness of the nylon-6 layers from 10 to 5 nm in Ti-PNCs had little effect on k, but k increased in Ag+Ti-PNCs significantly due to an increase in the effective volume fraction of Ag in the 5 nm thick nylon-6 layer, enhancing the nano-capacitor network effect.

4   Experimental

4.1   Fabrication

Ti and nylon-6 based capacitors were fabricated via layer-by-layer deposition of five individual layers of metal(s) and nylon-6 in an Edwards Auto 306 Cryo evaporator at a base pressure of 5x10^{-4} Pa. Titanium wire (99.7% pure, Alfa Aesar, 0.25 mm diameter), nylon-6 (Aldrich), and aluminum wire (99.999% pure, Alfa Aesar, 0.5 mm diameter) were thermally evaporated onto a glass slide sequentially using different W boats. The top and bottom (1st and 5th) layers of Al (40 nm each) formed the electrodes of a simple parallel-plate capacitor. These samples are referred to as Ti$_i$-Ny$_t$ where the subscripts i and t are variables which denote the deposition rate of Ti and the final thickness of the nylon-6

layer respectively. A schematic of the five alternate layers formed during evaporation is shown in Figure S3 (see Supporting Information).

Ag (99.99% pure, Advent, 0.125 mm diameter), Ti and nylon-6 based capacitors were fabricated similarly by tandem deposition of nine individual layers as shown in Figure 8. These samples are referred to as Ag+Ti$_i$-Ny$_t$. The deposition rates i of Al, nylon-6, and Ag were maintained at 0.5, 0.1, and 0.1 nm/s in all experiments.

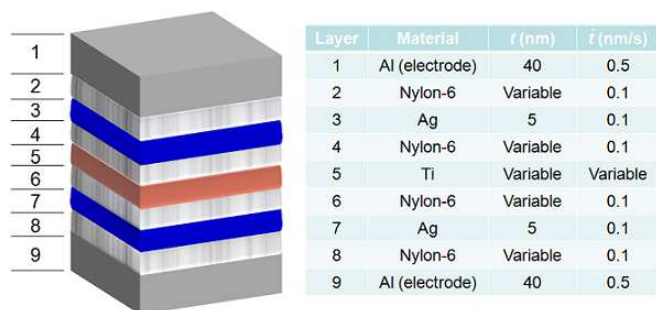| Layer	Material	t (nm)	$\dot{t}$ (nm/s)
1	Al (electrode)	40	0.5
2	Nylon-6	Variable	0.1
3	Ag	5	0.1
4	Nylon-6	Variable	0.1
5	Ti	Variable	Variable
6	Nylon-6	Variable	0.1
7	Ag	5	0.1
8	Nylon-6	Variable	0.1
9	Al (electrode)	40	0.5

Fig. 8 A schematic of alternate layers of Al, Ag, Ti and nylon-6.

4.2 Characterisation

The growth of the Ti and Ag layers were studied in a JEOL 3000F transmission electron microscope operating at 300 kV. In order to obtain images with both atomic number Z-contrast and diffraction-contrast, STEM was carried out at a relatively low angle. The features in some SAED patterns were enhanced through the adjustment of levels using the "HDR" plug-in in ImageJ/Picasa image processing software. All processed images are referred to as "enhanced" images and presented alongside the original images. Preparation of TEM samples and dielectric studies were carried out as described in sections TEM and Impedance spectroscopy in Supplementary Information.

Acknowledgements

References

1 A. C. Balazs, T. Emrick and T. P. Russell, *Science*, 2006, **314**, 1107.

2 H. Tang, Y. Lin, C. Andrews and H. A. Sodano, *Nanotechnology*, 2011, **22**, 015702.

3 P. Barber, S. Balasubramanian, Y. Anguchamy, S. Gong, A. Wibowo, H. Gao, H. Ploehn and H. Loye, *Materials*, 2009, **2**, 1697.

4 W. U. Huynh, J. J. Dittmer and A. P. Alivisatos, *Science*, 2002, **295**, 2425.

5 J. C. Grunlan, A. R. Mehrabi, M. V. Bannon and J. L. Bahr, *Advanced Materials*, 2004, **16**, 150.

6 X. Zhao, A. A. Koos, B. T. T. Chu, C. Johnston, N. Grobert and P. S. Grant, *Carbon*, 2009, **47**, 561.

7 Q. He, T. Yuan, X. Zhang, X. Yan, J. Guo, D. Ding, M. A. Khan, D. P. Young, A. Khasanov, Z. Luo, J. Liu, T. D. Shen, X. Liu, S. Wei and Z. Guo, *Journal of Physical Chemistry C*, 2014, **118**, 24784.

8 J. Zhu, S. Wei, N. Haldolaarachchige, D. P. Young and Z. Guo, *Journal of Physical Chemistry C*, 2011, **115**, 15304.

9 X. Zhang, X. Yan, Q. He, H. Wei, J. Long, J. Guo, H. Gu, J. Yu, J. Liu, D. Ding, L. Sun, S. Wei and Z. Guo, *ACS Applied Materials & Interfaces*, 2015, **7**, 6125.

10 C. Pecharroman and J. S. Moya, *Advanced Materials*, 2000, **12**, 294.

11 X. Huang, P. Jiang and L. Xie, *Applied Physics Letters*, 2009, **95**, 242901.

12 Z. M. Dang, Y. H. Lin and C. W. Nan, *Advanced Materials*, 2003, **15**, 1625.

13 C. Huang, Q. M. Zhang and J. Su, *Applied Physics Letters*, 2003, **82**, 3502–3504.

14 Y. Song, T. W. Noh, S. Lee and J. R. Gaines, *Physical Review B*, 1986, **33**, 904.

15 D. M. Grannan, J. C. Garland and D. B. Tanner, *Physical Review Letters*, 1981, **46**, 375.

16 F. He, S. Lau, H. L. Chan and J. Fan, *Advanced Materials*, 2009, **21**, 710.

17 Y. Shen, Y. Lin, M. Li and C.-W. Nan, *Advanced Materials*, 2007, **19**, 1418.

18 T. Wei, C. Q. Jin, W. Zhong and J. M. Liu, *Applied Physics Letters*, 2007, **91**, 222907.

19 Y. Zhang, Y. Wang, Y. Deng, M. Li and J. Bai, *ACS Applied Materials & Interfaces*, 2012, **4**, 65.

20 W. Benhadjala, I. Bord-Majek, L. Bechou, E. Suhir, M. Buet, F. Rouge, V. Gaud, B. Plano and Y. Ousten, *Applied Physics Letters*, 2012, **101**, 142901.

21 A. Mahadevegowda, N. P. Young and P. S. Grant, *Nanotechnology*, 2014, **25**, 475706.

22 Y. U. Wang, D. Q. Tan and J. Krahn, *Journal of Applied Physics*, 2011, **110**, 044103.

23 J. W. Xu and C. P. Wong, *Applied Physics Letters*, 2005, **87**, 082907.

24 Y. Niu, Y. Bai, K. Yu, L. He, F. Xiang and H. Wang, *Journal of*

Nanoscale Accepted Manuscript

Materials Research, 2013, **28**, 2644.

25 J. Y. Kim, H. S. Jung, J. H. No, J.-R. Kim and K. S. Hong, *Journal of Electroceramics*, 2006, **16**, 447.

26 J. Li, S. I. Seok, B. Chu, F. Dogan, Q. Zhang and Q. Wang, *Advanced Materials*, 2009, **21**, 217.

27 B. Babuji, C. Balasubramanian and M. Radhakrishnan, *Journal of non-crystalline solids*, 1983, **55**, 405.

28 Q. Cheng, W. Ahmad, G. Liu and K. Wang, 11th IEEE International Conference on Nanotechnology, 2011, p. 1598.

29 W. G. Lee, S. I. Woo, J. C. Kim, S. H. Choi and K. H. Oh, *Thin Solid Films*, 1994, **237**, 105.

30 T. Busani and R. Devine, *Semiconductor Science and Technology*, 2005, **20**, 870.

31 A. Mahadevegowda, N. P. Young and P. S. Grant, *Journal of Physics: Conference Series*, 2014, **522**, 012041.

32 Y. Zou, Z.-A. Wang, X.-H. Lan, N.-K. Huang and C.-F. Wang, *Journal of the Korean Physical Society*, 2009, **55**, 2650.

33 A. K. Srivastava, M. Deepa, S. Bhandari and H. Fuess, *Nanoscale Research Letters*, 2009, **4**, 54.

34 D. Shectman, D. Vanheerden and D. Josell, *Materials Letters*, 1994, **20**, 329.

35 Y. Zhang, M. Ma, N. Gu, L. Xu and K. J. Chen, *Chinese Chemical Letters*, 2004, **15**, 1005.

36 W. Wei, X. Mao, L. A. Ortiz and D. R. Sadoway, *Journal of Materials Chemistry*, 2011, **21**, 432.

37 G. J. Kovacs and P. S. Vincett, *Journal of Colloid and Interface Science*, 1982, **90**, 335.

38 G. J. Kovacs, P. S. Vincett, C. Tremblay and A. L. Pundsack, *Thin Solid Films*, 1983, **101**, 21.

39 Y. P. Khanna, W. P. Kuhn and W. J. Sichina, *Macromolecules*, 1995, **28**, 2644.

40 C. von Bechtolsheim, V. Zaporojtchenko and F. Faupel, *Applied Surface Science*, 1999, **151**, 119.

41 Q. M. Zhang, H. F. Li, M. Poh, F. Xia, Z. Y. Cheng, H. S. Xu and C. Huang, *Nature*, 2002, **419**, 284.

42 Z.-M. Dang, T. Zhou, S.-H. Yao, J.-K. Yuan, J.-W. Zha, H.-T. Song, J.-Y. Li, Q. Chen, W.-T. Yang and J. Bai, *Advanced Materials*, 2009, **21**, 2077.

43 H. Takele, H. Greve, C. Pochstein, V. Zaporojtchenko and F. Faupel, *Nanotechnology*, 2006, **17**, 3499.

44 D.-W. Kim, D.-H. Lee, B.-K. Kim, H.-J. Je and J.-G. Park, *Macromolecular Rapid Communications*, 2006, **27**, 1821.

45 Z. M. Dang, L. Z. Fan, Y. Shen and C. W. Nan, *Chemical Physics Letters*, 2003, **369**, 95.

Nanoscale Accepted Manuscript